Chemical 3D-imaging of glass inclusions from allende (CV3) olivine via SIMS: A new insight on chondrule formation conditions

L. Florentin, Etienne Deloule, F. Faure, D. Mangin

CHEMICAL 3D-IMAGING OF GLASS INCLUSIONS FROM ALLENDE (CV3) OLIVINE via SIMS: A NEW INSIGHT ON CHONDRULE FORMATION CONDITIONS.

L. Florentin[1], E. Deloule[1,] F. Faure[1], D. Mangin[2]
[1]CRPG, UMR CNRS 5873, (Université de Lorraine BP20, 54501, Vandœuvre les Nancy, FRANCE),
[2]IJL, UMR CNRS 7198 (Université de Lorraine, Parc de Saurupt, 54000 Nancy, FRANCE)

Corresponding author: florentinlea@gmail.com

Abstract

Natural glass inclusions - hosted in Mg-rich olivines from Allende (CV3) type I chondrules - and synthetic melt inclusions - trapped in forsterite crystallized from CMAS (CaO-MgO-Al_2O_3-SiO_2) melts - were mapped by Secondary Ion Mass Spectrometry (SIMS) for CMAS major oxides. The first ever 3D chemical images of extra-terrestrial glass inclusions were obtained, along with chemical depth profiles for each oxide. Results show similar patterns for both synthetic glass inclusions (trapped in olivine formed by slow crystallization in a magmatic liquid) and natural inclusions from Allende's olivines. No incompatible-rich boundary layer or diffusion pattern was observed in either case. The absence of an incompatible-rich boundary layer suggests that the olivine overgrowth surrounding glass inclusions in Allende's olivines was formed during slow cooling of the host olivine and likely the surrounding chondrule. This provides new constraints on the cooling rates of type I chondrules.

1. Introduction

Chondrules are silicate blebs embedded, with Ca-Al rich inclusions (CAIs) and metal drops, in a fine-grained matrix of variable porosity. Together, they represent the main components of the undifferentiated meteorites that are chondrites (*Sears and Dodd, 1988; Zanda, 2004, Connolly and Jones, 2016 and references therein*). Chondrules measure between 100 µm and 1 cm in diameter and display a wide range of textures, from glassy to porphyritic. They are thought to have formed by brief and repeated phases of heating (*Hewins and Radomsky, 1990*). Porphyritic chondrules are often studied because they correspond to approximately 85% of all chondrule textural types in ordinary chondrites (*Gooding and Keil, 1981*). They are usually composed of olivines and pyroxenes. They can be classified according to either their redox state or their

mineralogy. The focus of this study is the "type I" chondrules, i.e. chondrules whose silicates have low Fe-Ni contents. In this case, the olivines are forsteritic (i.e. Mg-rich). Both PO (Porphyritic Olivine) and POP (Porphyritic Olivine and Pyroxene) chondrules were studied. The origin of type I chondrules is still under debate (*Grossman and Larimer, 1974; Wasson, 1993; Yu and Hewins, 1998; Connolly and Desch, 2004; Alexander et al., 2008; Chaussidon et al., 2008; Asphaug et al., 2011; Sanders and Scott, 2012; Fedkin and Grossman, 2013; Johnson et al., 2015, Florentin et al., 2017*). In order to understand how chondrules formed, it is necessary to understand the processes that form the minerals they host, in particular olivines.

Any approach aimed at understanding the formation and behavior of olivine within the chondrules requires study of the glass inclusions they host. These glass inclusions are liquid blebs trapped inside the host minerals during mineral growth (*Roedder, 1979*). Such glass inclusions were observed inside olivines from chondrules in early studies (*Sorby, 1864; Dodd, 1969*). The inclusions are isolated and ovoid and may host a shrinkage bubble and sometimes daughter minerals (*Fuchs et al., 1973*). These petrological features are also typical of primary terrestrial melt inclusions (*Roedder, 1981*), suggesting that inclusions from terrestrial and extraterrestrial samples could behave similarly as a recorder of the growth-environment of their olivine hosts.

Experimental work on olivine formation (*Donaldson, 1976; Jambon et al., 1992; Pack and Palme, 2003; Schiano, 2003; Faure and Schiano, 2005)* established that melt inclusions (i.e. glass inclusions with a magmatic origin) may not necessarily be representative of the bulk magma from which they originate, depending on the process that controls the olivine growth: diffusion or interface attachment (screw dislocation, surface nucleation or continuous growth mechanisms). When cooling rates are slow, olivine grows by interface attachment processes: diffusion of the components in the melt to and from the melt / olivine interface is fast relative to the uptake and rejection of components at the interface (*Faure and Schiano, 2005*). Consequently, the liquid trapped within an olivine to constitute the melt inclusion is representative of the original melt. In contrast, when a crystal grows rapidly, olivine growth is controlled by diffusion, and melt inclusions should trap a compositional boundary layer that develops at the crystal-liquid interface. If so, skeletal or dendritic olivine will be produced. The chemical composition of the inclusions will not in this case be representative of the bulk initial melt composition, even if the inclusion is experimentally re-homogenized. The entrapped melt

inclusions will in fact be enriched in slowly diffusing incompatible elements rejected from the olivine structure, such as Al and, to a lesser extent, Ca.

Inclusions hosted in Mg-rich olivines from type I chondrules have been extensively studied over the last few decades (*Fuchs et al., 1973; Grossman and Clark, 1978; Kurat et al., 1997; Varela et al., 2002; 2005; 2006; Varela and Kurat, 2009, Faure et al., 2012*). Glass inclusions can be separated into four groups based on their chemical composition: Al-rich, Al-poor, Na-rich, and Si-rich (*Varela et al., 2002, Faure et al., 2017*). Varela *et al*. (*2002*) considered these chemical compositions to be "exotic", meaning that they are not in equilibrium with their host olivine. More recently, it was shown that the exotic compositions recorded in Al-rich glass inclusions hosted in Mg-rich olivines could be reproduced experimentally by slow growth of olivine from a CMAS liquid (*Faure et al., 2012*). According to Faure and Tissandier (*2014*), the exotic compositions observed inside synthetic melt inclusions result from metastable crystallization of olivine in near-equilibrium conditions on the walls of the inclusions. This suggests that, like for terrestrial melt inclusions, the original magma compositions of exotic glass inclusions hosted in Mg-rich olivines of chondrules can be experimentally determined or recalculated. However, this requires that, again as with terrestrial inclusions, the natural extraterrestrial inclusions did not trap a compositional boundary layer during their formation.

A study of inclusions from Semarkona type II chondrules by nanoSIMS showed that a two-micron chemical zoning was present at the inclusion-olivine interface (*Tronche et al., 2007*). However, no such data exist for type I chondrules, whose origin is presently under debate. To answer this important question, we perform a comparative study of synthetic melt inclusions trapped in olivine grown slowly under controlled conditions (*Faure and Tissandier, 2014*) and natural glass inclusions from the Allende (CV3) meteorite. Both inclusion types were studied in 3D via SIMS in order to construct 3D chemical images of the inclusions. From these, chemical depth profiles of the inclusions can be drawn, to allow investigation of the presence of a boundary layer at the glass inclusion / host olivine interface.

Though 2D high-resolution imaging via SIMS was developed many years ago (*Levi-Setti et al., 1987*), no study has so far applied it to the chemical 3D-imaging of melt inclusions. Today, many techniques allow 2D or 3D chemical imaging, but only the ion probe, using depth profiles, provides, a resolution high enough to distinguish an expected few tens of nanometer scale heterogeneity for non-conductive materials (*Adams and Barbante, 2012*). Furthermore, in

contrast with the lateral profiling proposed by *Tronche et al., 2007,* 3D chemical imaging allows us to ensure that no daughter crystal is present in the inclusion. Consequently, this study is also an opportunity to develop an analytical protocol for mapping inclusions in 3D via SIMS.

2. Analytical methods

2.1. Sample preparation

Three synthetic glass inclusions were selected from olivines experimentally produced by slowly cooling a CMAS liquid in a vertical furnace (charge number 16 in *Faure and Tissandier, 2014*). The starting glass material (47.32 wt. % SiO_2, 11.96 wt. % Al_2O_3, 12.21 wt. % CaO, 28.48 wt. % MgO) was chosen to represent the compositions of the primordial planetesimals that could produce Al-rich glass inclusions hosted in type I porphyritic olivine chondrules (*Faure et al., 2012*). The starting material was first heated for 1 h at 1540°C (4°C above the liquidus temperature) and then cooled slowly at 2°C h^{-1} to 683°C (below the glass transition).

Three natural glass inclusions were selected from thick sections of Allende (CV3) meteorite. Two of the glass inclusions were sampled from two distinct olivines hosted in two type I chondrules and the other inclusion came from an isolated olivine. The olivines selected exhibited no clear petrological indications of alteration (no sign of Fe penetration within the chondrule or olivine, Fo# above Fo90). The chemical compositions of the glass inclusions and their host olivine crystals are available in *Appendix 1*. Careful observation allowed us to select only inclusions that met previously established pristine criteria (*Roedder, 1979*): isolated, with a retraction bubble and an ovoid shape, no visible leak, and no proximity of a fracture. They were also selected only when glassy (i.e. no devitrification or visible daughter crystal) (*Figure 1*). Each inclusion was brought to the surface by polishing with corundum discs. For the purpose of 3D mapping via Secondary Ion Mass Spectrometer (SIMS), only inclusions with sizes of between 3 and 20 µm were considered. Each inclusion was then carbon coated and observed using SEM in order to confirm its glassy nature and to roughly estimate its chemical composition. It is worth noting that gold coating is not usually performed on meteorite samples because Au cannot be fully removed. Therefore, both natural and synthetic samples were carbon coated for this study.

2.2. SIMS analyses

As the four CMAS oxides (Al_2O_3, SiO_2, MgO and CaO) account for 88 to 98 wt. % of the whole inclusion composition for Allende inclusions (as calculated from major element data for glass inclusions from Allende; *Florentin et al., 2017*), only these four elements were analyzed. Analyses were performed using the CAMECA IMS 1280 at CRPG, Nancy (France) and the CAMECA IMS 7F at IJL, Nancy, (France).

The elements were measured at the masses of $^{24}Mg^{16}O$, $^{28}Si^{16}O$, $^{27}Al^{16}O$, $^{40}Ca^{16}O$ for analyses with the CAMECA IMS 7f. For the CAMECA IMS 1280, elements were measured at the masses of ^{26}Mg, ^{27}Al, ^{30}Si, ^{40}Ca and $^{24}Mg^{16}O$, $^{28}Si^{16}O$, $^{27}Al^{16}O$, $^{40}Ca^{16}O$. All masses were measured for each sample in order to select the best signal and minimize the risk of C interferences. For both ion probes, a 10 kV Cs^+ primary ion beam was used to obtain a small beam size of ≈ 300 nm with a current intensity varying from 130 to 200 pA during measurements. Although a smaller beam would have provided a better lateral resolution, it would not have allowed abrasion of enough matter to measure the whole depth of the inclusion within a reasonable length of time. The secondary ions images were acquired by ion counting on EM in monocollection mode, with each individual image consisting of 256×256 pixels.

For analysis with the CAMECA IMS 1280, the secondary ions were accelerated at 10kV (impact energy at 20 keV) and a mass resolution at 5000. In contrast, with the CAMECA IMS 7F, the secondary ions were accelerated at 5kV (impact energy at 15 keV). The lower impact energy provides a better depth resolution, but the mass resolution of 4000 for the secondary ions is not enough to separate major elements or oxides from carbon interferences.

Each mass (including the background) was measured for 10 seconds with a waiting time of 1 second. This resulted in a cycle lasting around 2 minutes and sputtering of between 15 and 30 nm depth.

As stated in the previous section, each inclusion was brought to the surface of the sample and then analyzed with SEM. Afterwards, the whole remaining inclusion (i.e. the part below the surface) was sputtered in order to collect 3D chemical images. Each cycle provided a 2D chemical image with an area of between 20x20 and 30x30 µm, depending of the inclusion size,

corresponding to sputtering of 30 to 15 nm depth. A chemical 3D image of the sample was then obtained by stacking the 2D images. Depending on the inclusion size and depth, the total number of cycles for one inclusion varied between 200 and 2000. This resulted in acquisitions lasting from two to more than twenty-four hours, depending on the settings of the probe and the size of the inclusion. The acquisition time was estimated from the inclusion size and the settings, but as inclusions were sputtered from thick sections (which did not allow us to observe the 3D shape of the inclusion), each analysis was carefully monitored.

The 3D images and depth profiles were collected using the WinImage® and Wincurve® software provided by CAMECA. For each acquired cycle, (i.e. a 2D-image that represents a few tens of nanometers) each pixel on the image contained counting information for the concerned element. Chemical depth profiles for an inclusion were extracted by compiling, for each cycle, data from an area drawn manually on the image of the inclusion (*Figure 2a and 2b*). After analysis, the depth pits were measured using a Nikon Eclipse LV100 optical microscope, calibrated using a Moticam 3000 Camera.

Each depth profile is presented as an oxide/silica ratio in order to account for eventual internal shift from the probe. All data were also normalized using the oxide/SiO_2 ratio of the host olivine, measured using an SEM (JEOL JSM-6510) equipped with a Brucker Quantax EDS, for consistency. Analyses on EDS were calibrated following the protocol detailed in Florentin et al., 2017.

3. Results

Results are presented in the form of 3D images of half glass inclusions (*Figure 2b*). The color scale of the 3D images corresponds to the number of atoms counted per pixel of the image. Because of the rounded shape of the inclusion and the beam size of about 300 nm, the periphery of the inclusion is depleted in Al relative to its center due to the contribution of the surrounding olivine, which contains no Al. By selecting an area of 1x1 to 2x2 µm size at the center of the inclusion, it is possible to combine the counting for all the pixels in the area, for each element and for each level between the surface and the bottom of the inclusion. The data are reported as AlO/SiO MgO/SiO and CaO/SiO ratios and are normalized to the oxide/SiO_2 mass ratios

measured via SEM for the olivine. In this way, it was possible to draw depth profiles for the oxide/SiO_2 ratios. It is worth noting that for all inclusions, the duration and the number of acquired cycles of the depth profile depends on the size of the inclusion.

Profiles from all inclusions typically display three distinct segments. Based on the 3D-imaging, the first can be attributed to the inclusion and the last to olivine The intermediate segment corresponds to the transition zone between glass and crystal.

3.1 Study of chemical profiles at glass inclusion-host olivine interface from synthetic samples

Details of 3D images and depth profiles for each synthetic inclusion are available in *Appendix 2*. (For SEM and optical microscopic images of these inclusions, see *Faure and Tissandier, 2014*). Typical depth profiles for two synthetic inclusions are presented in *Figure 3*, one measured with the IMS 7F ion probe, the other with the IMS 1280 ion probe. Both inclusions are hosted in the same synthetic olivine. The two profiles show three distinct segments.

Inclusion 1, analyzed with the IMS 7F ion probe, shows a nearly flat CaO profile with a CaO/SiO_2 ratio of around 0.01. This flat pattern is most likely due to isobaric interferences between CaO and C_2O_2, caused by carbon coating, whose signals were not separated due to the low mass resolution of the IMS 7F settings. The Al_2O_3/SiO_2 ratio decreases from 0.1 to 0.002, and is higher in the melt inclusion than in the olivine. MgO measurements were not used because of the isobaric interference of C_2O on MgO due to the carbon coating of the section. Because of the low mass resolution of the IMS 7F setting, it was not possible to separate the two signals. For this inclusion (inclusion 1), the transition zone between glass and olivine is not clearly separated from the melt inclusion signal. This is due to the small size of the inclusion: the sputtering removed 2.5 µm in depth but the bottom of the inclusion was at around 1.5 µm depth below the surface. The signal, especially for Al_2O_3/SiO_2, does not correspond to a straight line that drops when the end of the inclusion is reached, but rather to a smooth slope towards the end of the inclusion. As the inclusion is small and rounded (i.e. the bottom of the inclusion is not flat), the signal recorded from the inclusion decreases gradually. The depth profile for the Al_2O_3/SiO_2 ratio thus shows a slight decrease towards the glass/olivine transition. The profile is flat in the olivine and shows a steeper slope at the interface. Inclusion 2 was analyzed with the IMS 1280 ion probe. The CaO/SiO_2 ratio remains around 0.03 and slowly decreases towards the bottom of the inclusion. This value is higher than the value measured in inclusion 1, even though they

contain the same amounts of CaO and SiO_2. This slight difference is most likely due to the fact that the measurements were made using two different ion probes. The MgO/SiO_2 ratio for inclusion 2 is clearly an artifact due to a matrix effect: the emission yield of MgO relative to SiO is different and is higher for a glass than for an olivine.

The Al_2O_3/SiO_2 ratio depth profile shows the three distinct segments: a gently decreasing slope inside the inclusion, a flat profile in the olivine, and a steep slope in the transition zone.

If we take into account the 1 µm size difference between the two inclusions, these results show that the depth profiles are similar for both inclusions in spite of the use of two different SIMS.

3.2 Study of chemical profiles in inclusions hosted in olivine from Allende chondrite

Details of 3D images and depth profiles for natural glass inclusions from Allende are available in *Appendix 2*. The depth profiles measured on two inclusions are presented in *Figure 4*. These are representative of the analyses of three Allende glass inclusions. Inclusions were analyzed from two distinct olivines with the 1280 ion probe. The chemical depth profiles show the typical three distinct segments: largely flat in the glass inclusion, flat in the olivine, and sloped in the steep transition zone. Both inclusions show the same ratios of MgO/SiO_2 and CaO/SiO_2 and the inclusion "Allende 1" shows a lower Al_2O_3/SiO_2 ratio than the inclusion "Allende 2". This reflects the large compositional range of Allende inclusions (*Florentin et al., 2016*), and is consistent with Al-rich and Al-poor glass inclusions groups defined previously (*Varela et al., 2002*). It can also be observed that these profiles have a much better definition than the profiles of synthetic inclusions. This is due to the diameter of the inclusions (15 to 20 µm for natural inclusions, 3 to 5 µm for synthetic inclusions).

Likewise, the slopes at the transition zone of the natural inclusions seem to be much steeper than those of the synthetic inclusions, but this is an effect of the total depth of analysis.

3.3 Data processing

3.3.1 Expected chemical compositions at the glass/olivine interface

The elemental profiles recorded in the glass inclusions depend on the processes involved in the olivine growth. Three types of chemical profile can be expected at the periphery of the inclusion (*Figure 5*). (i) If olivine growth is controlled by interface processes, a flat profile will be

expected in the glass (*Figure 5a*). In this case, the olivine and the liquid are at equilibrium or near equilibrium conditions at all times. (ii) If the olivine grows rapidly, the growth is therefore controlled by diffusion processes and an increase in incompatible elements in the glass should be recorded towards the glass–olivine transition zone (*Figure 5b*). In this case, Al and Ca, both incompatible elements with regard to olivine, are not incorporated into the olivine and a boundary layer can be observed at the periphery of the inclusion. (iii) Finally, when melting of the olivine walls occurs around the inclusion, a decrease in the incompatible elements should be observed due to their enrichment in the olivine component (*Figure 5c*). In this case, Mg and Si would be added to the liquid composition, which would increase the MgO content and decrease the Al_2O_3 and CaO contents in the glass towards the transition zone.

It is now possible to compare these theoretical profiles with our measured profiles from the synthetic and natural inclusions. However, it is worth noting that theoretical profiles, unlike measured ones, are free of any matrix effect. The measured profiles for MgO, CaO, AlO and SiO, depend on the matrix (olivine or glass) they are measured in. Consequently, the ratios cannot be quantitatively representative of the real chemical ratios within the inclusion or the olivines, which are shown for the theoretical profiles.

Our results show no increase in incompatible elements, which rules out the possibility of an incompatible-rich boundary layer due to rapid crystallization trapped in the inclusion. They instead suggest a decrease in incompatible elements.

This could indicate reheating of the inclusion after trapping and melting of olivine on the walls of the inclusion. However, several arguments suggest this is not a reasonable hypothesis. (1) Synthetic and natural inclusions both contain only a few wt. % MgO. In the case of olivine melting, the MgO content of the inclusion would increase dramatically, which is not observed here. (2) Both synthetic and natural glass inclusions show very similar profiles. However, the thermal history of synthetic inclusions is well known, and they were not reheated after the trapping of the inclusions (*Faure and Tissandier, 2014)*. (3) Calcium diffuses more than two times faster than Al in silicate melts (*Liang et al., 1996*). Consequently, the Al_2O_3/CaO ratio is expected to show the existence of an incompatible-rich boundary layer, as the amount of Al_2O_3 should rise relative to the amount of CaO near the transition zone. Thus, in the case of such a boundary layer, the Al_2O_3/CaO ratio should increase towards the wall of the inclusion due to diffusion. When compared, Al_2O_3/CaO ratios for synthetic inclusions and Allende natural glass

inclusions (*Figure 6*) show a similar evolution at the transition zone, with only a slight dependence on the inclusion size.

3.3.2 Analytical artifact or real chemical transition?

For synthetic inclusions, Al_2O_3/SiO_2 ratio patterns display two distinct segments from the center of the inclusion towards the border of the olivine: a nearly flat profile inside the inclusion and a steep slope at the transition zone (*Figure 3*). However, the corresponding theoretical profile (Figure 5a) shows no transition zone. The transition zone can thus be attributed to analytical artifacts. (1) The main part of this artifact is the shape of the glass inclusion. As the bottom of the inclusion is not flat but rounded, the abundances (recorded over an area) would be expected to decrease slowly towards the end of the inclusion, as a growing part of the area becomes olivine (for details, see *Appendix 3*). (2) Another cause of the artifact is due to a technical limitation, in that depth profiles are calculated from an area rather than a discrete point. As seen in *Figure 7*, the size of the mixing zone between the olivine and the inclusion can be related to the size of the area (*Figure 7a*) used to draw depth profiles from the stacking of 2D images: the smaller the area, the smaller the mixing zone (*Figure 7c*). However, a small area corresponds to a mean calculated from fewer pixels, which increases the noise in the depth profile (see Areas 1 and 2 in *Figure 7b*). Consequently, in order to obtain a well-defined profile, it is necessary to use an area that is wide enough to prevent noise but small enough to achieve the smallest possible mixing zone. (3) Furthermore, it was established that when sputtering, the beam implants some atoms further into the sample instead of removing them (*Wilson et al., 1989*). The tail effect associated with this ion mixing is usually considered to be a hundred nanometers in size, which is much smaller than the mixing area, even if in our case the very high contrast of Al contents in the melt inclusion and in the olivine might enhance the tail depth.

Consequently, the progressive decrease in incompatible elements observed at the olivine-glass inclusion interface is the result of an analytical artifact and does not correspond to an incompatible-rich boundary layer. As such, it will be considered an artifact in the following discussion.

4. Discussion

4.1 Profiles comparison between synthetic glass inclusions and natural glass inclusions from Allende

At the transition zone, the Al_2O_3/CaO ratio depth profiles from synthetic and natural melt inclusions (*Figure 6*) show similar patterns: a slight decrease when reaching the inclusion walls, a steep decrease in the transition zone, and then a flat profile in the olivine. The synt1 and synt 2 profiles resemble each other closely but are not identical. This may be attributed to the fact that the inclusions are not of the same size, meaning that the size of the transition zones are different. It could also be due to the use of different probes with different settings. The two profiles obtained from the Allende inclusions (All1 and All2) also do not superimpose. In this case, the differences can be attributed to the wide compositional range of the glass inclusions in natural samples. Nevertheless, all four profiles display the same overall trend, with a transition zone smaller than 2 µm. The nature of this transition zone will be discussed in the following sections.

4.2 Implications for the absence of an incompatible-rich boundary layer

Al_2O_3/CaO ratios (*Figure 6*) suggest that both natural and synthetic glass inclusions experienced a similar process of formation. If true, then the inclusions were not affected by the complex history of the meteorite. Several reasons can be invoked to explain this. First, chondrules do not record the occurrence of any high temperature event after their formation. The formation of the parent body and potential alteration events took place at much lower temperatures, and thus only affected the parent body on a local scale. As the olivines were selected from Allende thick sections that showed no petrological evidence of alteration, we can assume that they did not suffer significantly from low temperature alteration. Consequently, the glass inclusions, sealed within the olivine, should not have suffered any low temperature alteration. Collisions between chondrite parent bodies should also leave their marks, especially in terms of thermal changes. For this reason, olivines were also only selected when they looked pristine and when the fine-grained matrix surrounding the chondrules was non-metamorphosed.

Analogy between synthetic and natural glass inclusions suggests that glass inclusions hosted in olivines from the Allende chondrite could have formed by slow crystallization of a molten planetesimal, as proposed by *Faure et al. (2012)*. In this case, the olivine crystals would have grown slowly enough to trap, in the inclusions, the chemical composition of their growth environment. Thus, any post-trapping processes such as daughter mineral crystallization, olivine overgrowth, or formation of a shrinkage bubble, should be reversible. The problem of iron loss sometimes observed for terrestrial melt inclusions (*Danyushevsky et al., 2002*) should not be an issue here as the olivine crystals are extremely magnesian-rich and were extracted from type I chondrules in which Fe is in a reduced form. This suggests that experimental homogenization of these inclusions should allow the retrieval of the composition of the parent magma to olivine crystals (Tissandier et al., 2017).

4.3 Insight on olivine growth rate and chondrule cooling rate

The Al_2O_3/CaO ratio within glass inclusions hosted in chondrule olivines has been investigated in previous studies (*Varela et al., 2002; Varela et al., 2005*). The majority of glass inclusions record a chondritic ratio in spite of Ca and Al disparities from one inclusion to another. The authors suggest that this chondritic ratio, in association with Al and Ca variability, corresponds to a diffusion process, and propose a rapid crystallization. Data from Varela and coworkers (*2009 and reference therein*) show that some inclusions also contain high amounts of Na_2O (up to 15 wt. %). Data show that these Na-rich inclusions are also depleted in CaO and record a different Al_2O_3/CaO ratio to the chondritic ratio. However, if diffusion is due to rapid crystallization, Ca and Na should diffuse in the same direction. Hence, if there is an increase in Na, an increase in Ca should also be observed. This rapid crystallization process thus remains questionable.

In the present study, no chemical gradient is observed at the interface between inclusions and olivines hosted in chondrules.

This suggests that the olivine overgrowth was not rapid and was therefore not controlled by diffusion processes. Consequently, the last high-temperature cooling episode of the olivine, which probably corresponds to formation of the chondrule, was slow enough that the olivine overgrowth, inside the inclusion, was not controlled by diffusion. Thus, the cooling of the

chondrule was slower than Ca and Al diffusion. Furthermore, Ca zoning would be expected within the olivine overgrowth because the Ca content of liquid inclusion increases during crystallization (*Libourel, 1999; Spandler and O'Neill, 2010*). However, no such variation can be observed in the olivine surrounding the inclusions, neither in the experimental nor the Allende olivines (see *Figure 3*). Consequently, the cooling rate of the olivine (and likely that of the whole chondrule) must have been at least as slow as the cooling rate used in the experiments (2°C/h) and inevitably slower than the diffusion rate of Al in the liquid and Ca in olivine to erase all chemical profiles. Furthermore, the absence of an incompatible-rich boundary layer at the olivine / glass inclusion interface also allows the inclusion to be considered as having recorded the environment of host-olivine growth. As detailed in the introduction to this paper, if an inclusion has not recorded an incompatible-rich boundary layer, its chemical composition can yield information on the growth environment and / or processes of the host olivine.

As explained earlier in this paper, Ca and Al have different diffusion rates. If we consider that olivines were formed in a molten planetesimal with a chondritic composition (as suggested in *Florentin et al., 2017*), then the CaO/Al_2O_3 ratio should be close to the chondritic ratio as Ca and Al are both incompatible elements. Consequently, if olivine growth had been controlled by diffusion, i.e. that it had undergone rapid crystallization, then the CaO/Al_2O_3 ratio should be fractionated and thus not correspond to the chondritic ratio. The CaO/Al_2O_3 ratio remains close to the chondritic ratio (≈ 0.7 when calculated with data from *Anders and Grevesse, 1989*) for both the glass inclusions measured in this study (0.64) and the majority of glass inclusions analyzed in the literature (0.79) (see Florentin et al., 2017 for a compilation). This suggests that there was also no incompatible-rich boundary layer in the inclusion when it was first trapped during olivine formation. Thus, as for chondrules, olivine growth in a molten planetesimal imposes a slow cooling rate. Similarly, the cooling rate of the olivine in the molten planetesimal is necessary low and, in particular, is slower than Ca and Al diffusion rates. It should therefore theoretically be possible to determine the minimum time (i.e. a maximum cooling rate) required to erase Ca zoning on the rim of olivine overgrowth around the inclusion.

Diffusion coefficients are not easily calculated. Experiments were carried out by Coogan et al. (2005) on both San Carlos olivines and forsterites in order to determine the relationship between fO_2, temperature T, and diffusion coefficient D for Ca along the three axes of the olivine ([100], [010], [001]), as a function of temperature and oxygen fugacity fO_2. The authors proposed the

best fits for pre-exponential term Do and E for each axis. The diffusion coefficient D at a given T and fO_2 is then defined by the Arrhenius equation (1):

$$\log (D) = \log [Do\ e^{(-E/RT)}] + 0.31\ \Delta \log fO_2 \quad (1)$$

However, this equation is dependent on many variable parameters. The fO_2 can be determined from previous studies of type I chondrules, rich in magnesian olivine (log (fO_2) from -9 to -13 according to *Lauretta et al., 2001*). D is strongly dependent on temperature. In this study, we focus on a temperature of 900 °C, close to the end of olivine overgrowth crystallization. This temperature was deduced from the compositions of glass inclusions (*Faure and Tissandier, 2014*). For Coogan and co-workers, E was calculated to be 193 kJ/mol but previous papers showed that for highly magnesian olivines, E could be as high as 400 kJ/mol (*Hain, 1998; Morioka, 1981*). The variability of E has a critical effect on the final value of D. Thus, it seems difficult to establish a precise D value for our samples, but typical cooling times can be estimated from the available range of D, and the duration of Ca diffusion along 1 µm of olivine, the estimated size of the overgrowth rim around inclusion, can then be calculated, from equation (2):

$$\sigma = \sqrt{Dt} \quad (2)$$

where σ is the typical diffusion distance, set to 1 µm.

Diffusion is a dynamic process, and is fast at high temperature, and slow at low temperature, as suggested by the large range of diffusion coefficients: at low temperature with respect to olivine melt, D ranges from $1.4\ 10^{-17}$ m²/s at 1200°C (*Morioka, 1981*) to $2.0\ 10^{-20}$ m²/s at 900°C (*Coogan et al., 2005*). For log(D) values in the range of -20 to -18, Ca diffusion along 1 µm will require between 10^6 and 10^8 s (12 days to 3 years). The longer times are probably overestimated, as our synthetic olivines were formed in 21 days (*Faure and Tissandier, 2014*) and do not show any limit layer.

We therefore believe that the growth of the natural olivine occurred under conditions close to those of the experimental olivine growth described in *Faure and Tissandier, 2014*, with a cooling rate of 2°C/h.

To summarize, the olivines appear to have grown slowly via interface attachment processes in a magma from a molten planetesimal and have trapped glass inclusions that recorded information

on the olivine surroundings (*Figure 8a*). Afterwards, an impact event (*Sanders and Scott, 2012*) ejected these olivines into the protoplanetary disk, along with gas, liquid and dust (*Figure 8b*). Interactions between gas, liquids and solid resulted in the formation of proto-chondrules (*Figure 8c*). It is now acknowledged that proto-chondrules underwent several heating episodes (*Zanda, 2004 and references therein*), as did the olivines they host (*Figure 8d*). Consequently, heating episodes allowed the olivine overgrowth inside glass inclusions to melt and re-crystallize sequentially. As no incompatible-rich boundary layer is recorded in the present glass inclusions, this suggests that the last cooling episode to have affected the olivines (and therefore the chondrules) was slow enough to have allowed Ca diffusion in olivine.

5. Conclusion

This study presents the first high resolution (a few tens of nm) chemical 3D-images and depth profiles of glass inclusions. Comparison of synthetic inclusions trapped in slow growing olivine via a magmatic process and of natural glass inclusions from Allende chondrite shows that synthetic and natural samples behave similarly, especially concerning the absence of an incompatible-rich boundary layer at the walls of inclusions. This suggests that both types of olivine (synthetic or from chondrules) were formed by the same process and that their growth was controlled by interface attachment processes. This in turn suggests that olivines, and likely, chondrules, cooled more slowly than the diffusion rate of Al in melt from glass inclusions, allowing olivine overgrowth to form slowly and maintain a metastable equilibrium with its surrounding glass inclusion. Furthermore, as the inclusions display a chondritic CaO/Al_2O_3 ratio, this means that no diffusion process occurred during growth of olivine. Consequently, the host olivine probably grew slowly, at a cooling rate slower than Ca and Al diffusion rates.

Acknowledgements

We want to thank our editor Sara Russell for her insightful comments. We also wish to thank Alan Rubin, Dominique Hezel and an anonymous reviewer for their thorough reviews and constructive advice. Many thanks to Alice Williams for revising the English. This study was supported by the Programme National de Planétologie: PNP-INSU.

References:

Adams, F., Barbante, C., 2012. History and present status of imaging analysis. *Talanta*. **102**, 16–25. doi:10.1016/j.talanta.2012.06.057

Alexander, C.M.O'D., Grossman, J.N., Ebel, D.S., Ciesla, F.J., 2008. The formation conditions of chondrules and chondrites. *Science*, **320**, 1617-1619. doi: 10.1126/science.1156561

Anders E. and Grevesse N. (1989) Abundances of the elements: Meteoritic and solar. *Geochim. Cosmochim. Acta* **53**, 197–214.

Asphaug, E., Jutzi, M., Movshovitz, N., 2011. Chondrule formation during planetesimal accretion. *Earth Planet. Sci. Lett.* **308,** (3-4), 369–379. doi:10.1016/j.epsl.2011.06.007

Chaussidon, M., Libourel, G., Krot, A.N., 2008. Oxygen isotopic constraints on the origin of magnesian chondrules and on the gaseous reservoirs in the early Solar System. *Geochim. Cosmochim. Acta*. **72**, 1924-1938.

Connolly, H.C.Jr, Desch, S.J., 2004. On the origin of the "kleine Kügelchen" called Chondrules. *Chem. Erde.* **64**, 95-125.

Connolly, H.C. Jr., Jones, R.H., 2016. Chondrules: the canonical and noncanonical views. *J. Geophys. Res. Planets.* **121**, 1885-1899, doi: 10.1002/2016JE005113

Coogan, L. A., Hain, A., Stahl, S., Chakraborty, S., 2005. Experimental determination of the diffusion coefficient for calcium in olivine between 900°C and 1500°C. *Geochim. Cosmochim. Acta.* **69(14)**, ,3683-3694.

Danyushevsky, L.V., McNeill, A.W., Sobolev, A.V., 2002. Experimental and petrological studies of melt inclusions in phenocrysts from mantle-derived magmas: an overview of techniques, advantages and complications. *Chem. Geol.* **183***,* 5-24.

Donaldson, C., H., 1975. Calculated diffusion coefficients and the growth rate of olivine in a basalt magma. *Lithos*, **8,** 163-174.

Donaldson C., H., 1976. An experimental investigation of olivine morphology. *Contrib. Mineral. Petrol.* **57**, 187–213.

Dodd, R.T., 1969. Metamorphism of the ordinary chondrites: A review. *Geochim. Cosmochim. Acta*, **33**, 161-203.

Faure, F., Schiano, P., 2005. Experimental investigation of equilibration conditions during forsterite growth and melt inclusion formation. *Earth Planet. Sci. Lett.* **220**, 331-344.

Faure, F., Tissandier, L., 2014. Contrasted liquid lines of descent revealed by olivine-hosted melt inclusions and the external magma. *J. Petrol.* **55**, 9, 1779-1798.

Faure, F., Tissandier, L., Florentin, L., Devineau, K., 2017. A magmatic origin for silica-rich glass inclusions hosted in porphyritic magnesian olivines in chondrules: an experimental study. *Geochim. Cosmochim. Acta*. **204**, 19-31.

Faure, F., Tissandier, L., Libourel, G., Mathieu, R., Welsch, B., 2012. Origin of glass inclusions hosted in magnesian porphyritic olivines chondrules: Deciphering planetesimal compositions. *Earth Planet. Sci. Lett.* **319-320**, 1-8.

Florentin, L., Faure, F., Tissandier, L., Deloule E., Lequin, D., 2017. Origin of Na in glass inclusions hosted in olivine from Allende CV3 and Jbilet Winselwan CM2: implications for chondrule formation. *Earth Planet. Sci. Lett.* **474**, 160-171.

Fedkin, A.V., Grossman, L., 2013. Vapor saturation of sodium: Key to unlocking the origin of chondrules. *Geochim. Cosmochim. Acta*. **112**, 226-250.

Fuchs, L.H., Olsen, E., Jensen, K.J., 1973. Mineralogy, Mineral-Chemistry, and Composition of the Murchison (C2) Meteorite. *Smithsonian Contrib. to Earth Sci.* **10**, 1-39.

Gooding, J.L., Keil, K., 1981. Relative abundances of chondrule primary textural types in ordinary chondrites and their bearing on conditions of chondrule formation. *Meteoritics*. **16**, 1, 17-43.

Grossman, L., Clark, S.P. Jr., 1978. High-temperature condensates in chondrites and the environment in which they formed. *Geochim. Cosmochim. Acta*. **37**, 635-649.

Grossman, L., Larimer, J.W., 1974. Early chemical history of the solar system. *Rev. Geophys. Space Phys.* **12**, 1, 71-101.

Hain, A., 1998. ^{42}Ca Tracer diffusion in Olivin in Abhängigkeit von der Temperatur, dem Sauerstoffpartialdruck und der chemischen Zusammensetzung, Ph. D Dissertation, Fachbereich Chemie der Justus Liebig Universität Gießen, Gießen, Germany.

Hewins, R.H, Radomsky, P.M., 1990. Temperature conditions for chondrule formation. *Meteoritics*. **25**, 309-318.

Jambon, A., Lussiez, P., Clocchiatti, R., Weisz, J., Hernandez, J., 1992. Olivine growth rates in a tholeiitic basalt: An experimental study of melt inclusions in plagioclase. *Chem Geol,* **96**, 277–287.

Johnson, B.C., Minton, D.A., Melosh, H.J., Zuber, M.T., 2015. Impact jetting as the origin of chondrules. *Nature*. **517**, 339-341.

Kubicki, J., D., Muncill, G., E., Lasaga, A., C., 1990. Chemical diffusion in melts on the CaMgSi2O6-CaAl2Si2O8 join under high pressures. *Geochim. Cosmochim. Acta*, **54**, 2709-2715.

Kurat, G., Varela, M.E., Hoppe, P., Clocchiatta, R., 1997. Glass inclusions in Renazzo olivine: condensates from the solar nebula ? *60th Ann. meeting of the Met. Soc. Maui, U. S. A.*, #5194 (abstr.).

Lauretta, D. S., Buseck, P. R., Zega, T. J., 2001. Opaque minerals in the matrix of Bishumpur (LL3.1) chondrite: Constraints on the chondrule formation environment. *Geochim. Cosmochim. Acta*. **65(8)**, 1337-1353.

Levi-Setti, R., Chabala, J.M., Wang, Y.L., 1987. Aspects of high resolution imaging with a scanning ion microprobe. *Ultramicroscopy*. **24**, 97-114.

Liang, Y., Richter, F.M., Davis, A.M., Watson, E.B., 1996. Diffusion in silicate melts: I. Self diffusion in CaO-Al_2O_3-SiO_2 at 1500°C and 1 GPa. *Geochim. Cosmochim. Acta.* **60**, 4353-4367.

Libourel, G., 1999. Systematics of calcium partitioning between olivine and silicate melt: implications for melt structure and calcium content of magmatic olivines. *Contrib Mineral Petrol.* **136**, 63-80.

Morgan, Z., Liang, Y., Hess, P., 2006. An experimental study of anorthosite dissolution in lunar picritic magmas: Implications for crustal assimilation processes. *Geochim. Cosmochim. Acta.* **70**, 3477-3491.

Morioka, M., 1981. Cation diffusion in olivine - II. Ni-Mg, Mn-Mg, Mg and Ca. *Geochim. Cosmochim. Acta.* **45,** 1573–1580.

Pack, A., Palme, H., 2003. Partitioning of Ca and Al between forsterite and silicate melt in dynamic systems with implications for the origin of Ca, Al-rich forsterites in primitive meteorites. *Meteorit. Planet. Sci.* **38**, 1263–1281.

Roedder E., 1979. Origin and significance of magmatic inclusions. *Bull. Minéral.* **102**, 487-510.

Roedder, E., 1981. Significance of Ca-Al-rich silicate melt inclusions in olivine crystals from the Murchison type II carbonaceous chondrite. *Bull. Minéral.* **104**, 339-353.

Sanders, I.S., Scott, E.R.D., 2012. The origin of chondrules and chondrites: Debris from low-velocity impacts between molten planetesimals? *Meteorit. Planet. Sci.* **12**, 2170-2192.

Schiano, P., 2003. Primitive mantle magmas recorded as silicate melt inclusions in igneous minerals, *Earth Sci. Rev.* **63**, 121–144.

Sears, D.W.G., Dodd, R.T., 1988. Overview and classification of meteorites, in *Meteorites and the early solar system* (eds. J.F. Kerridge , M. Shapley Matthews). The university of Arizona press, Tuscon. 3-31.

Sorby, H.C, 1864. On the microscopical structure of meteorites. *Proc. Roy. Soc. Lond. A XIII.* #333 (abstr.).

Spandler, C., O'Neill, H. St.C., 2010. Diffusion and partition coefficients of minor and trace elements in San Carlos olivine at 1,300°C with some geochemical implications. *Contrib Mineral Petrol.* **159**, 791-818. DOI 10.1007/s00410-009-0456-8

Tronche, E., Reinhardt, P., Mostefaoui, S., Guilhaumou, N., Robert, F., 2007. Melt inclusions in olivine crystals from chondrules: New insights from nanoscale concentration profiles in the Semarkona chondrite. *C. R. Geosci.* **339**, 667-673.

Varela, M.E., Kurat, G., Hoppe, P., Brandstätter, F., 2002. Chemistry of glass inclusions in olivines of the CR chondrites Renazzo, Acfer 182 and El Djouf 001. *Geochim. Cosmochim. Acta.* **66**, 1663-1679.

Varela, M.E., Kurat, G., Zinner, E., 2005. A liquid-supported condensation of major minerals in the solar nebula: Evidence from glasses in the Kaba (CV3) chondrite. *Icarus*. **178**, 553-569.

Varela, M.E., Kurat, G., Zinner, E., 2006. The primary liquid condensation model and the origin of barred olivine chondrules. *Icarus*. **184**, 344-364.

Varela, M. E., Kurat, G., 2009. Glasses in meteorites and the Primary Liquid Condensation model. *Mitt. Österr. Miner. Ges.* **155**, 279-320.

Wasson, J.T., 1993. Constraints on chondrule origins. *Meteoritics.* **28**, 14-28.

Wilson, R.G., Stevie, F.A., Magee, C.W., 1989. Secondary Ion Mass Spectrometry. 2.1-1. *New-York: Wiley*.

Yu, Y., Hewins, R.H., 1998. Transient heating and chondrule formation: Evidence from sodium loss in flash heating simulation experiments. *Geochim. Cosmochim. Acta.* **62**, 159-172.

Zanda, B., 2004. Chondrules. *Earth Planet. Sci. Lett.* **224**, 1-17.

Zhang, Y., Ni, H., Chen, Y., 2010. Diffusion date in silicate melts. *Reviews in Min. Geoch.* **72**, 311-408.

Captions for each figure:

Figure 1: SEM (BSE) image of glass inclusion Allende 3 inside its host olivine.

Figure 2: Microscopic photography of a synthetic melt inclusion and 3D-images of AlO inside the inclusion obtained via SIMS.
The color scale for the 3D images corresponds to the number of atoms counted per pixel of the image. For all three images, the scale is in µm.
a: Synthetic inclusion observed in transmitted light. Next to it is the matching surface image (one cycle of acquisition) measured for Al by CAMECA IMS-1280. The atom counting area used to draw the corresponding depth profile is also shown (black square).
b. 3D-image of AlO for the synthetic inclusion shown in Figure 1a. The bubble appears as a slight decrease in AlO.
c: 3D-image of AlO for the same inclusion, slightly rotated, and including the volume corresponding to the area used to draw a depth profile.

Figure 3: Depth profiles for Al_2O_3/SiO_2, CaO/SiO_2 and MgO/SiO_2 ratios in two synthetic inclusions.
Inclusion 1 was measured with 7F IMS (top) and Inclusion 2 with 1280 IMS (bottom). The MgO/SiO_2 ratio can be observed for inclusion 2. Both Al_2O_3/SiO_2 ratio profiles show the typical three segments: a flat segment for the olivine, a smooth slope for the glass inclusion and a steep slope the transition zone.

Figure 4: Depth profiles for two inclusions from Allende chondrules.
Depth profiles for Al_2O_3/SiO_2, CaO/SiO_2 and MgO/SiO_2 ratios from two glass inclusions hosted in Allende chondrules, Allende 1 (a) and Allende 2 (b.). Both were measured with 1280 ion probe.

Figure 5: Sketches of theoretical depth profiles.
Sketches of theoretical depth profiles of Al_2O_3/SiO_2 (red), CaO/SiO_2 (green) and MgO/SiO_2 (blue) in glassy inclusion (GI) and in olivine.
(a.) olivine growth by interface attachment processes, (b.), rapid crystallization of the crystal and rejection of incompatible elements from the crystal in the liquid and (c.) fusion of the host olivine.
In each profile, the transition zone corresponds to the interface between the olivine and the inclusion. In profiles (b) and (c), the transition zone is marked by a chemical variation in incompatible elements. In profile (c), the transition zone is due to dissolution of olivine into the melt at the interface.

Figure 6: Shapes of Al_2O_3/CaO ratio depth profiles near the inclusion-olivine interface for both inclusion types.
Shapes of Al_2O_3/CaO ratio depth profiles near the inclusion-olivine interface in the two glass inclusions from Allende (All 1 and All 2) presented in *Figure 3* and in the two synthetic inclusions (Synth 1 and

Synth 2) presented in *Figure 2*. Only the inclusion-olivine interface is represented here to allow comparison of the behavior of Al_2O_3/CaO ratios.

Figure 7: Effect of the size of the area used to draw the depth profile on the size of the transition zone.
a: Chemical 2D-imaging (^{27}Al) of inclusion Allende 1. In the image, seven square areas were drawn in the center of the inclusion (marked by the red dashed line).
b: Al/Si depth profiles drawn from all seven square areas.
c: Same graph, showing the increasing size of the transition zone as a function of the increasing size of the square area.

Figure 8: Schematic drawing summarizing our model of olivine and chondrule formation and cooling rates.
a: Trapping of glass inclusions in slowly growing olivine within a molten planetesimal.
b: Ejection of olivines, gas, liquid and more generally dust during an impact event.
c: Interaction between olivine and the surrounding liquid and gas in order to form proto-chondrules.
d: After multiple heating episodes of the chondrule, a final phase of slow cooling allows the olivine overgrowth to grow back without forming a chemical boundary layer at the olivine / glass inclusion interface.

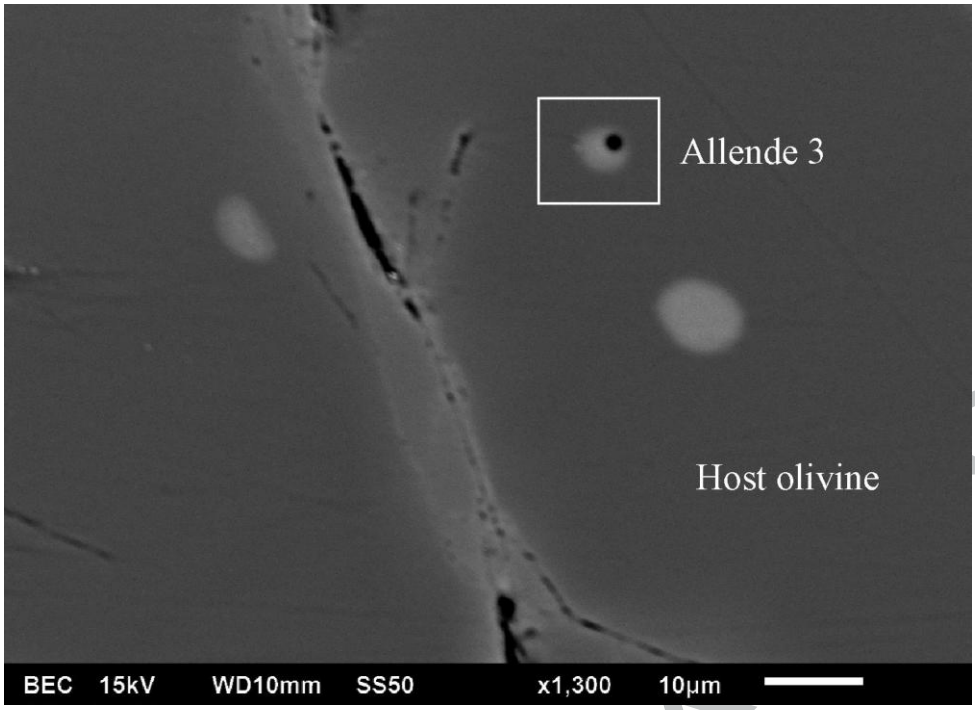

a.

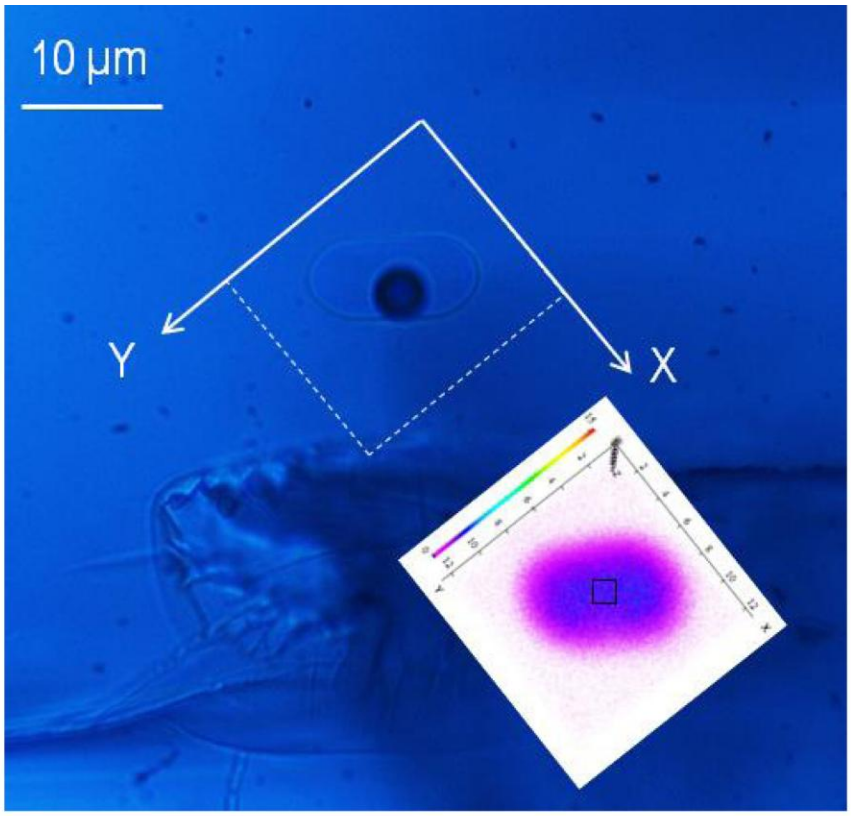
10 µm
Y
X

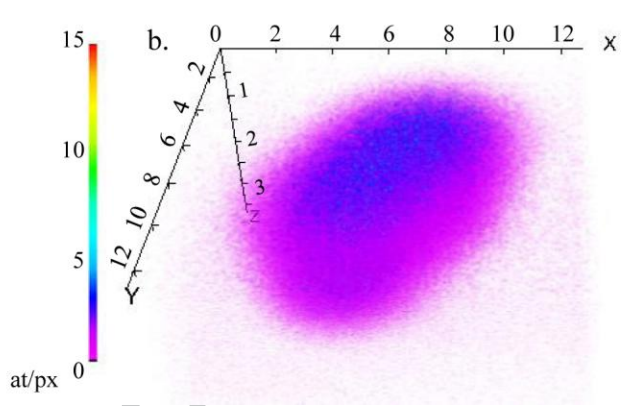
15
10
5
0
at/px
b.
0 2 4 6 8 10 12 X
2 4 6 8 10 12 Y
1 2 3 Z

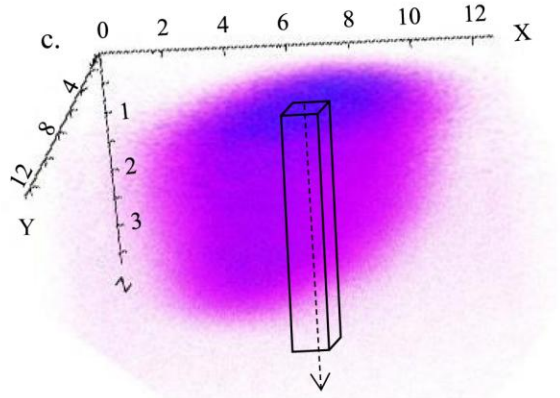
c.
0 2 4 6 8 10 12 X
4 8 12 Y
1 2 3 Z

a. Inclusion synt 1 - IMS 7F

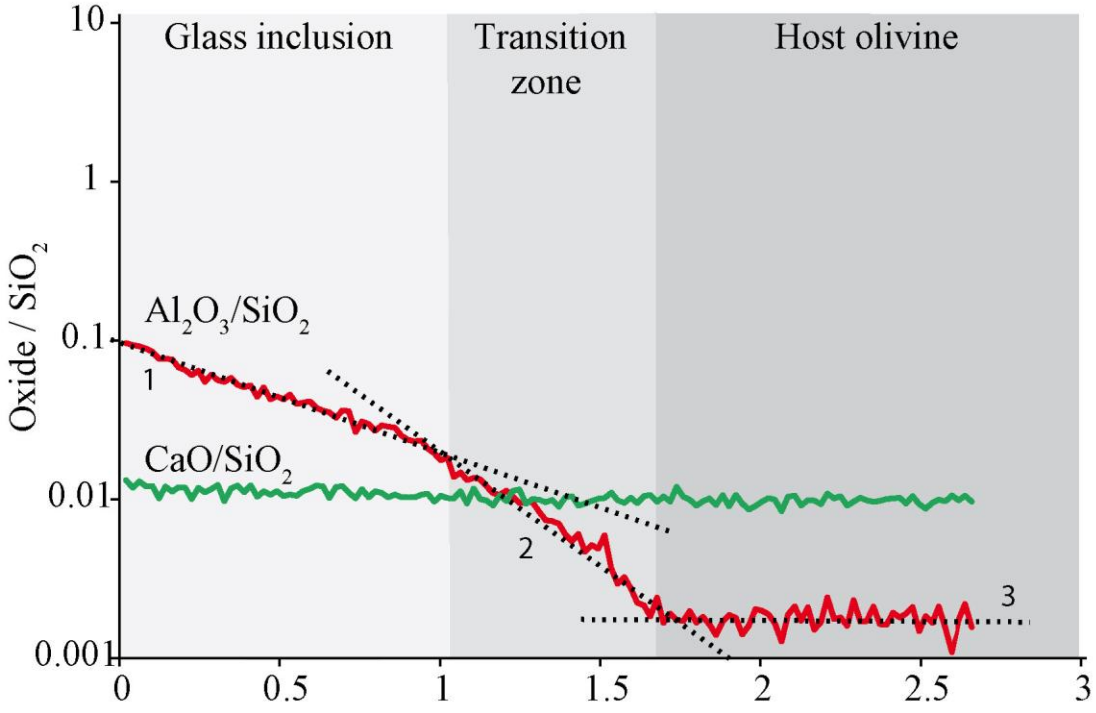

b. Inclusion synt 2 - IMS 1280

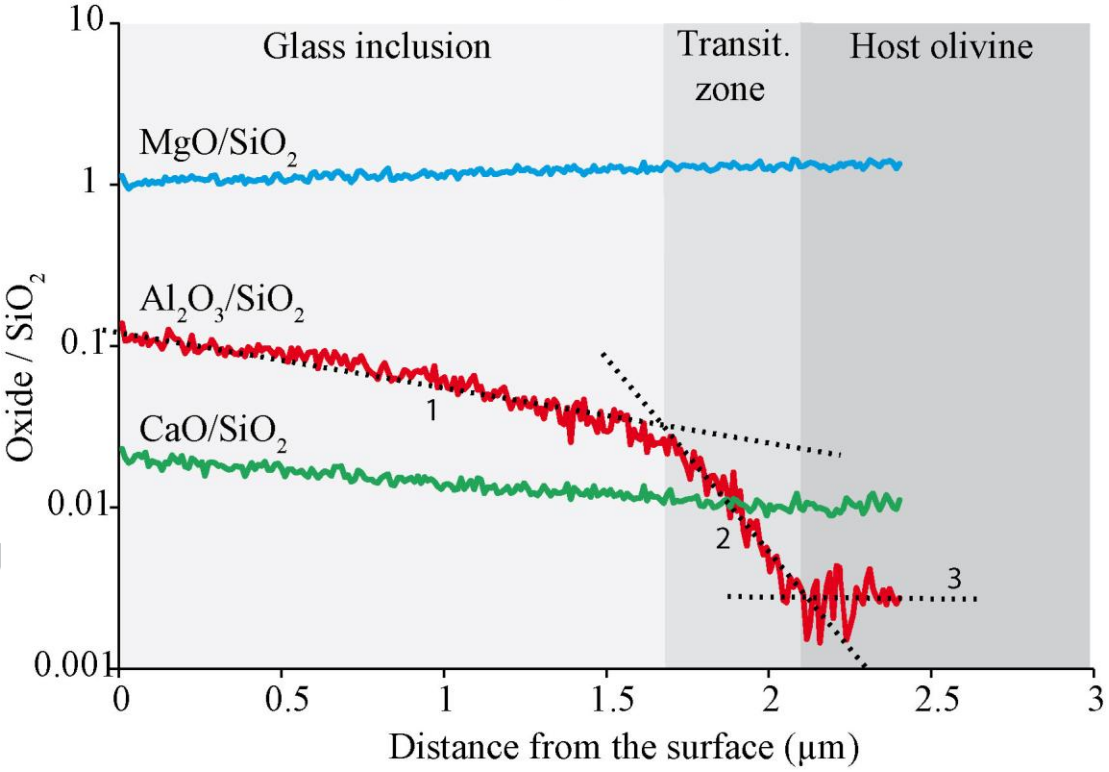

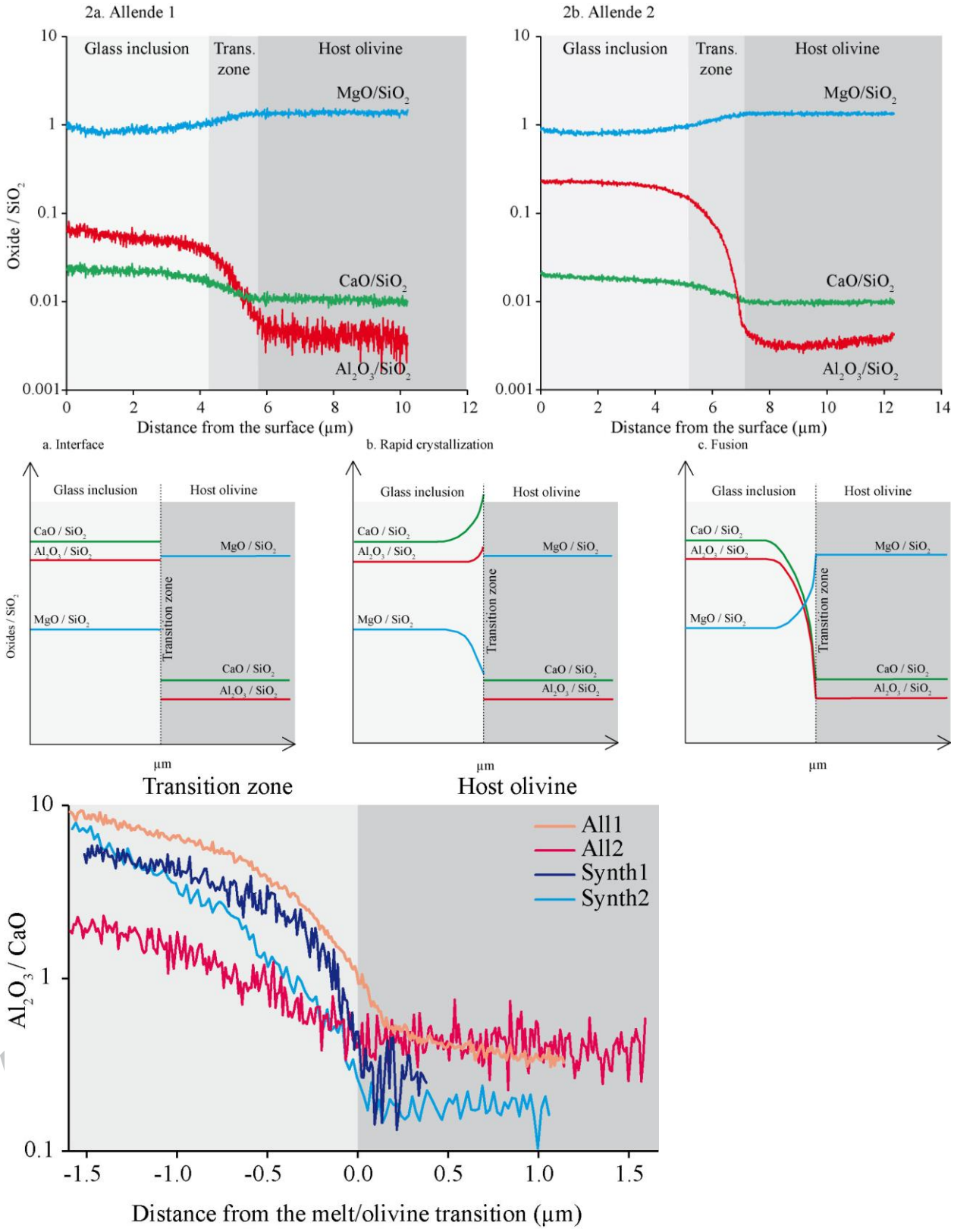
2a. Allende 1
2b. Allende 2
Glass inclusion
Trans. zone
Host olivine
MgO/SiO2
CaO/SiO2
Al2O3/SiO2
Oxide / SiO2
Distance from the surface (µm)
a. Interface
b. Rapid crystallization
c. Fusion
CaO / SiO2
Al2O3 / SiO2
MgO / SiO2
Transition zone
Oxides / SiO2
µm
Transition zone
Host olivine
All1
All2
Synth1
Synth2
Al2O3 / CaO
Distance from the melt/olivine transition (µm)

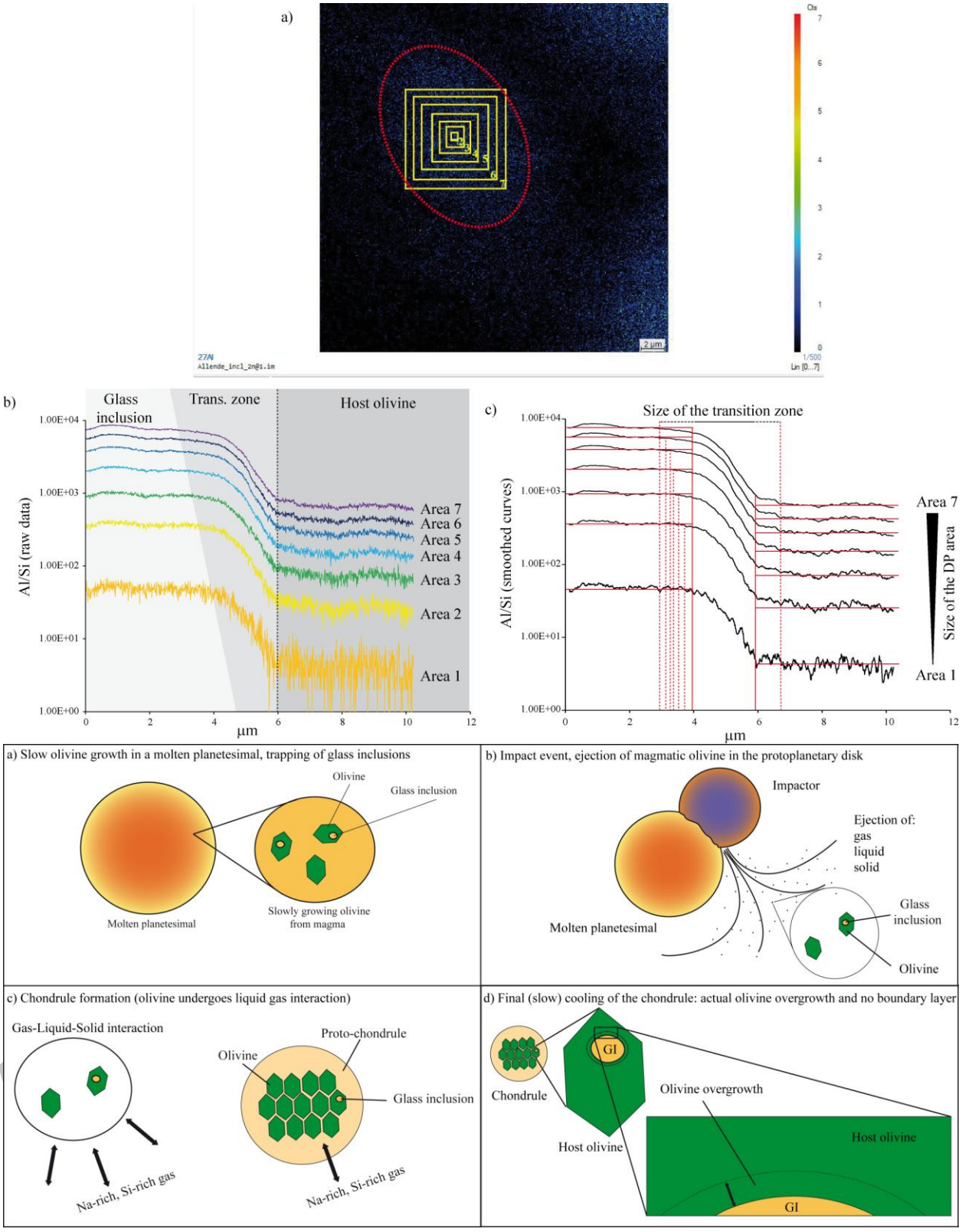
a)
Cts
7
6
5
4
3
2
1
0
1/500
Lin [0...7]
2 µm
27Al
Allende_incl_2n@1.im
b)
Glass inclusion
Trans. zone
Host olivine
Al/Si (raw data)
1.00E+04
1.00E+03
1.00E+02
1.00E+01
1.00E+00
0
2
4
6
8
10
12
µm
Area 7
Area 6
Area 5
Area 4
Area 3
Area 2
Area 1
c)
Size of the transition zone
Al/Si (smoothed curves)
Area 7
Size of the DP area
Area 1
a) Slow olivine growth in a molten planetesimal, trapping of glass inclusions
Olivine
Glass inclusion
Molten planetesimal
Slowly growing olivine from magma
b) Impact event, ejection of magmatic olivine in the protoplanetary disk
Impactor
Ejection of:
gas
liquid
solid
Molten planetesimal
Glass inclusion
Olivine
c) Chondrule formation (olivine undergoes liquid gas interaction)
Gas-Liquid-Solid interaction
Na-rich, Si-rich gas
Proto-chondrule
Olivine
Glass inclusion
Na-rich, Si-rich gas
d) Final (slow) cooling of the chondrule: actual olivine overgrowth and no boundary layer
GI
Chondrule
Olivine overgrowth
Host olivine
Host olivine
GI